http://dx.doi.org/10.21577/0103-5053.20180192

J. Braz. Chem. Soc., Vol. 30, No. 4, 727-735, 2019
Printed in Brazil - ©2019 Sociedade Brasileira de Química

Article

New Synthesis Method for a Core-Shell Composite Based on α-Bi_2O_3@PPy and its Electrochemical Behavior as Supercapacitor Electrode

Fárlon F. S. Xavier,[a] Carlos G. O. Bruziquesi,[b] Wélique S. Fagundes,[a] Elaine Y. Matsubara,[c] José M. Rosolen,[c] Adilson C. Silva,[b] Sheila C. Canobre[a] and Fábio A. Amaral[a]*

[a]*Laboratório de Armazenamento de Energia e Tratamento de Efluentes (LAETE), Instituto de Química, Universidade Federal de Uberlândia (UFU), Av. João Naves de Ávila, 2121, 38408-100 Uberlândia-MG, Brazil*

[b]*Laboratório de Química Tecnológica e Ambiental (LQTA), Instituto de Ciências Exatas e Biológicas, Universidade Federal de Ouro Preto (UFOP), 35400-000 Ouro Preto-MG, Brazil*

[c]*Departamento de Química, Faculdade de Filosofia, Ciências e Letras de Ribeirão Preto, Universidade de São Paulo, 14040-901 Ribeirão Preto-SP, Brazil*

New composite based on polypyrrole (PPy) and bismuth oxide (α-Bi_2O_3) was investigated as supercapacitor electrode. The α-Bi_2O_3 was obtained by hydrothermal route at 500 °C for 2 h. Cyclic voltammetry was used to electropolymerize PPy on graphite electrode (GE) or on GE/α-Bi_2O_3. The X-ray diffraction profile of Bi_2O_3 revealed the α-Bi_2O_3 monoclinic structure with space group $P2_1/c$. The scanning and transmission electron microscopy images showed that PPy coated α-Bi_2O_3. Raman spectra showed that PPy inhomogeneously coated α-Bi_2O_3, but it was still possible to obtain a α-Bi_2O_3@PPy core-shell hybrid composite with highly ordered α-Bi_2O_3 with electronic interaction between the oxide and the polymer chain of the polymer. The GE/α-Bi_2O_3@PPy composite electrode (type I supercapacitor) displayed a predominantly capacitive profile with low impedance values and good electrochemical stability after 50 charge and discharge cycles. The specific capacitance of α-Bi_2O_3@PPy composite was found in the range of 634 to 301 F g^{-1} to gravimetric current of 3 and 10 A g^{-1}, respectively.

Keywords: conducting polymers, bismuth oxide, supercapacitors, electrochemical devices

Introduction

Over the last years, core-shell structures based on oxide-oxide and oxide-polymer have been studied as interesting alternatives to produce composite materials with high specific capacitance. The CoO@MnO_2, NiO@MnO_2, TiO_2@MnO_2, Ag/polyaniline (PAni)@MnO_2, NiO@polypyrrole (PPy), and MnO_2@PPy composites are examples of core-shell structures, with specific capacitance as high as 1835 F g^{-1} at a current density of 1 A g^{-1}.[1-6] The present work investigated a core-shell structure prepared with two well-known materials: α-Bi_2O_3 and PPy.

α-Bi_2O_3 displays unique thermal and electrical transport properties and is easy to synthesize. This oxide is an interesting material for electrochemical applications: it can be employed as electrolyte or as the cathode of solid oxide fuel cells, not to mention its use in glasses and its photoconductive and thermoelectric applications.[7-12] In turn, PPy is an inexpensive, easy to prepare, environmentally friendly, and environmentally stable[13] conducting polymer with good electronic conductivity[14] and chemical stability; its specific capacitance can be tailored by altering its electronic structure.[14-19] PPy coatings can be obtained via low-cost chemical or electrochemical routes.

Supercapacitor development is a very important subject in the energy storage field. Supercapacitors have many applications that require high power and an extremely elevated number of discharge/charge cycles. Current batteries cannot fully meet the power requirements of the automotive, robotic, and the weather sectors.[9,20-22] So far, commercial supercapacitors have been unable to overcome the specific

*e-mail: fabioamaral@ufu.br

energy of traditional lead batteries (ca. 30-50 W h kg^{-1}), but core-shell materials could modify this scenario.

This paper reports on the fast and facile electrochemical synthesis of a graphite electrode (GE) containing adhered α-Bi_2O_3 coated with PPy as a core-shell granulated composite for use as high-performance supercapacitor electrode. In the GE/α-Bi_2O_3@PPy electrode, α-Bi_2O_3 and PPy serve as the "core" and the "shell" layer, respectively. The electrochemical behavior of the GE/α-Bi_2O_3@PPy hybrid electrode was evaluated by cyclic voltammetry (CV) and galvanostatic charge-discharge (GCD), to show that it can be applied as a supercapacitor with high specific capacitance in aqueous electrolytes.

Experimental

Sample preparation

α-Bi_2O_3 synthesis

All the chemical reagents were used without previous treatment. Typically, a given amount of bismuth(III) nitrate pentahydrate ($Bi(NO_3)_3.5H_2O$) was dissolved in ethylene glycol (EG) under constant magnetic stirring for 5 min. Then, the final solution was placed in a 200 mL Teflon-lined stainless steel autoclave at 140 °C for 2 h.[23] The liquid-solid mixture was centrifuged, to obtain a solid that was washed with water several times and dried in an oven at 80 °C for 3 h. An amorphous white powder was obtained. To achieve a crystalline material, the white powder was calcined in an oven at 500 °C for 2 h, to afford a yellow powder. The oxide was deposited on a vitreous carbon pellet (graphite) electrode by the dropping of an alcoholic α-Bi_2O_3 dispersion onto GE before electropolymerization of PPy on α-Bi_2O_3.

PPy electrochemical synthesis on GE and GE/α-Bi_2O_3

PPy was electropolymerized on the GE or GE/α-Bi_2O_3 surface by CV carried out from –0.30 to 0.90 V *vs.* $Ag_{(s)}/AgCl_{(s)}/Cl^-_{(aq)}$ at 50 mV s^{-1} in 50 mL of aqueous 1 mol L^{-1} KCl, containing previously distilled 0.01 mol L^{-1} pyrrole, up to total charge density of 150 mC cm^{-2} after 20 cycles for the GE/PPy electrode or after 8 cycles for the GE/α-Bi_2O_3@PPy hybrid electrode, respectively.

Structural and morphological characterization

X-ray diffractometry (XRD) was performed on a Shimadzu diffractometer (Model 6000; Cu Kα radiation λ = 1.5406 Å, voltage = 40 kV, current = 30 mA, scan rate = 1° min^{-1}, 2θ ranging from 20 to 70°). The unit cell parameters were calculated with the UnitCell Win program.[24] The diffractogram peaks had been previously adjusted with the Peak Fit software.[25]

The Raman spectroscopy measurements were performed on a Raman spectrometer (LabRAM HR Evolution) between 2000 and 200 cm^{-1} at room temperature, employing He-Ne ion laser of 1 mW with wavelength of 633 nm and charge couple device (CCD) detector with 1 cm^{-1} resolution.

The scanning electron microscopy (SEM) images were obtained with a Tescan SEM (Vega 3). The images were magnified 10,000 times; the acceleration voltage was 5 or 10 kV. The α-Bi_2O_3@PPy composite was also analyzed by high resolution (HR) electron transmission microscopy (TEM; JEOL 2100 TEM-MSC). For this purpose, α-Bi_2O_3@PPy particles were mechanically extracted from GE/α-Bi_2O_3@PPy electrode to make the HRTEM grid.

Electrochemical characterization

The capacitive performances of the GE/PPy, GE/α-Bi_2O_3, and GE/α-Bi_2O_3@PPy electrodes were tested by CV in 1 mol L^{-1} Na_2SO_4; a three-electrode system was used (GE/α-Bi_2O_3, GE/PPy, or GE/α-Bi_2O_3@PPy as the working electrode, GE as the counter electrode, and $Ag_{(s)}/AgCl_{(s)}/Cl^-_{(aq)}$ as the reference electrode). The electrochemical properties of the GE/α-Bi_2O_3, GE/PPy, and GE/α-Bi_2O_3@PPy electrodes were examined by CV, GCD, and electrochemical impedance spectroscopy (EIS). For the CV measurements, the electrodes were cycled from –0.30 to 0.70 V at 25 mV s^{-1}.

The GCD tests were carried out by the galvanostatic chronopotentiometry method. The tests were carried out from –0.30 to 0.70 V in 1 mol L^{-1} Na_2SO_4, at 3, 5, 10 and 20 A g^{-1}. The masses of all electrodes were about 0.10 mg. The mass employed in the determination of specific capacitance was obtained from the average mass of three electrodes prepared in similar conditions.

The EIS measurements were performed at an AC voltage, under open circuit voltage (OCV). The amplitude was 10 mV, and the frequency ranged from 10^4 to 10^{-1} Hz. The electrochemical tests were performed at room temperature. An Autolab potentiostat 302 N, interfaced with a microcomputer operating the software NOVA version 1.11, was employed.

Results and Discussion

α-Bi_2O_3 synthesis and structural characterization

$Bi(NO_3)_3.5H_2O$ dissolution in EG and heating at 140 °C for 2 h afforded the relatively stable $Bi_2(OCH_2CH_2O)_3$,[26]

a white powder (equation 1). Simultaneously, $Bi(NO_3)_3$ hydrolysis obtained white powder of $BiONO_3$ (equation 2).

$$2Bi(NO_3)_3.5H_2O_{(s)} + 3HOCH_2CH_2OH_{(l)} \rightarrow Bi_2(OCH_2CH_2O)_{3(aq)} + 6HNO_{3(aq)} + 10H_2O_{(l)} \quad (1)$$

$$Bi(NO_3)_{3(s)} + H_2O_{(l)} \rightarrow BiONO_{3(aq)} + 2HNO_{3(aq)} \quad (2)$$

The mixture of white powders, $Bi_2(OCH_2CH_2O)_3$ and $BiONO_3$, was calcined at 500 °C for 2 h to obtain Bi_2O_3, a yellow powder (equation 3).

$$Bi_2(OCH_2CH_2O)_{3(s)} + 2BiONO_{3(s)} + 7O_{2(g)} \rightarrow 2Bi_2O_{3(s)} + 6CO_{2(g)} + 2NO_{2(g)} + 6H_2O_{(g)} \quad (3)$$

The Bi_2O_3 XRD pattern (Figure 1a) displayed well-resolved and highly defined peaks and resembled the XRD pattern of the standard Joint Committee on Powder Diffraction Standards (JCPDS) No. 041-1449, indexed on the basis of a monoclinic structure, which attested that pure monoclinic α-Bi_2O_3[8] with space group $P2_1/c$ was formed. Figure 1b shows the α-Bi_2O_3 unit cell. The XRD of oxide synthesized through the solvothermal method did not have secondary diffraction peaks due to the use of EG, which acted as a chelating agent.[23,26] Moreover, EG significantly reduced the mobility of the different ion species in this medium. Additionally, EG served as a soft template that facilitated self-assembly of *in situ* grown microparticles through hydrogen bond formation, which controlled α-Bi_2O_3 crystal growth.[27]

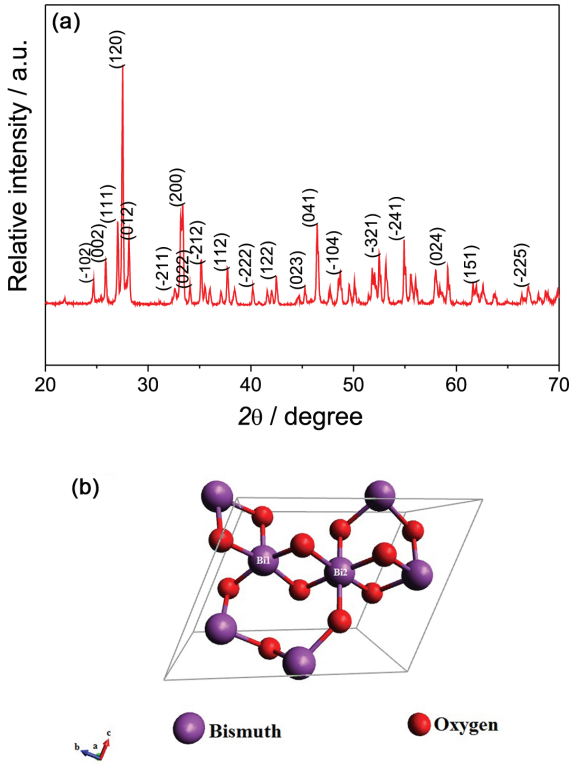

Figure 1. (a) XRD pattern and (b) unit cell of the α-Bi_2O_3.

The calculated unit cell parameters agreed with values reported for α-Bi_2O_3 (Table 1).[28]

Table 1. Unit cell parameters calculated for α-Bi_2O_3

	a / Å	*b* / Å	*c* / Å	*c* / *a*
This work	6.078	8.157	7.793	1.282
Literature[28]	5.850	8.165	7.510	1.284
JCPDS No. 041-1449	5.850	8.170	7.512	1.284

a, *b* and *c*: unit cell parameters; JCPDS: Joint Committee on Powder Diffraction Standards.

The unit cell parameters calculated herein were slightly higher than the unit cell parameters described in the literature, which was probably a consequence of the synthesis method. Nevertheless, the *c* / *a* ratio values (*c* / *a* = 1.282) were similar, which demonstrated that the unit cell was not distorted.

PPy electrochemical synthesis on the GE and GE/α-Bi_2O_3 electrodes

Figure 2 depicts the voltammograms recorded for PPy electrochemical synthesis on the GE and GE/α-Bi_2O_3 electrodes, as well as the GE/α-Bi_2O_3 electrode in 1 mol L^{-1} KCl in the absence of pyrrole monomers. Clearly, Figure 2a suggests a good stability of α-Bi_2O_3 on surface of GE, since the capacitive charge is the same at several cycles, while the voltammograms in Figures 2b and 2c show the increase of the anodic current density with increase in the number of cycles, evidencing the effective growth of the PPy on the GE and GE/α-Bi_2O_3 electrodes. In addition, Figure 2c revealed that PPy electrochemical synthesis on the GE/α-Bi_2O_3 electrode gave rise to a pair of redox peaks, which highlights the presence of a possible interaction between oxidized PPy (as verified on the Raman spectrum) and α-Bi_2O_3, which resulted in a material with favored electronic transfer.[29]

Thereby, the voltammograms due to PPy electrochemical synthesis on the GE/α-Bi_2O_3 electrode showed that fewer cycles (eight cycles) were necessary to achieve total charge as compared to PPy electrochemical synthesis on the GE electrode (20 cycles).

Raman characterization

It is well known in literature that the effect the doping of PPy can be investigated with Raman, such that eventual

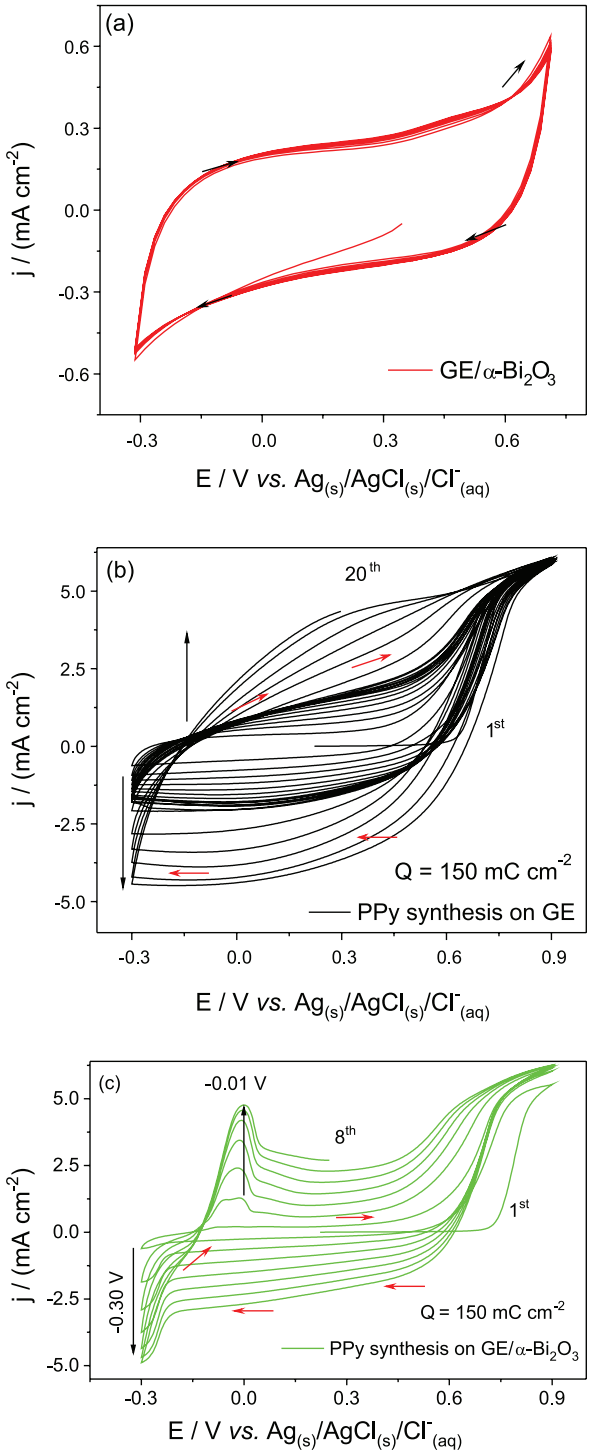

Figure 2. Cyclic voltammograms of the (a) GE/α-Bi_2O_3 electrode in 1 mol L^{-1} KCl; (b) PPy electropolymerized on the GE; and (c) PPy electropolymerized on the GE/α-Bi_2O_3 electrodes in 1 mol L^{-1} KCl containing 0.01 mol L^{-1} pyrrole monomer at 50 mV s^{-1}.

electronic interactions between PPy and α-Bi_2O_3 could be detected when present.[30] The GE Raman spectrum (Figure 3) displayed peaks at 1322 and 1568 cm^{-1}, which referred to the D-band and the G-band, respectively. The Raman spectrum of the GE/α-Bi_2O_3 electrode presented bands at 283 and 315 cm^{-1}, attributed to the bending modes of the BiO_5 and BiO_6 units, and bands at 410 and 449 cm^{-1}, which are due to the vibrational modes associated with a combination of Bi–O bond asymmetric stretching and bending modes.[31,32] It is worth to note that the oxide bands derived from GE/α-Bi_2O_3@PPy depend on the position of laser on sample. In the Raman spectrum of the GE/α-Bi_2O_3@PPy composite, there are two distinct regions: in one (red dashed line), the bands characteristic of the vibrational modes present in the existing bonds in Bi_2O_3 and PPy, and in another (black dotted line), the absence of bands of the Bi_2O_3, indicating an inhomogeneous coating of Bi_2O_3 by PPy.

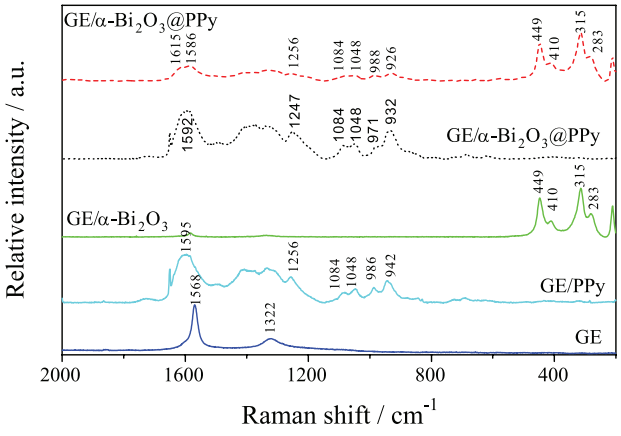

Figure 3. Raman spectra of the GE/α-Bi_2O_3, GE/PPy and GE/α-Bi_2O_3@PPy electrodes at two different regions of the electrode.

On the other hand, the Raman spectra of the GE/PPy and GE/α-Bi_2O_3@PPy electrodes in Figures 3b and 3c, in the region where the PPy bands are present, can be employed to detect the presence or not of expected electronic interaction between PPy and α-Bi_2O_3. In fact, the PPy Raman bands up and down shifts, which can be observed (Table 2), were associated with the PPy oxidation state. Thereby, Figure 2 shows that PPy was oxidized in Bi_2O_3@PPy. The double bands shown at about 1048 and 1084 cm^{-1} are initially assigned to be the C–H in plane deformation of oxidized PPy.[33] Table 2 summarizes the main vibrational modes of Raman spectra. Both Raman band intensities indicate predominance of the oxidized form of PPy and are related to higher conductivity values, corresponding to doping levels.

The Raman spectra presented in Figure 3, and the position of their bands summarized in Table 2, show greater presence of oxidized state (bipolaron) in the composite than in the PPy, suggesting greater conjugation of the polymer chain. Figure 3 also shows that bands at about 1595, 986 and 942 cm^{-1}, assignable to the reduced form, are still present in the most oxidized state due to the presence of a range of conjugation lengths in the composite film, but slightly displaced.[34] The oxide has an electron acceptor metal center

Table 2. Assignment of the peaks observed in the Raman spectra of the GE/α-Bi_2O_3, GE/PPy, and GE/α-Bi_2O_3@PPy electrodes[30-34]

Electrode	Raman shift / cm^{-1}	Assignment
GE/α-Bi_2O_3	449-280 315-283	Bi–O bond asymmetric stretching and bending modes bending modes of the BiO_5 and BiO_6 units
GE/PPy and GE/α-Bi_2O_3@PPy	1595 (1592)[a] 1314 and 1378 1256 (1247)[a] and 1047 986 (971)[a] and 942 (932)[a]	C=C symmetry stretching inter-ring (C–C) stretching C–H deformation mode ring deformation associated with dication and radical cation

[a]On the composite. GE: graphite electrode; PPy: polypyrrole.

(Lewis acid) from the PPy (Lewis base), weakening the bonds in the polymer chain, whose vibrational modes would be shifted to lower frequencies (superscript a in Table 2).

Raman analysis confirms the formation of p-n junction between PPy and oxide in core-shell structures, where electrons can be exchanged such that electrochemical answer of PPy can be influenced by the type of electronic structure of oxide.

Morphological characterization by SEM

Figures 4a-4c illustrate the morphology of the thin film of the GE/α-Bi_2O_3, GE/PPy, and GE/α-Bi_2O_3@PPy electrodes as analyzed by SEM. The SEM images of the GE/α-Bi_2O_3 electrode (Figure 4a) evidenced particles, which are aggregated in the shape of curved rods ranging from 2 to 5 μm, and individual spheroidal grains with average diameter around 70 nm. The thermal treatment applied on α-Bi_2O_3 to improve its crystallinity probably provoked a synthesis of α-Bi_2O_3 nanoparticles, which led to observed α-Bi_2O_3 microrods, the principal constituent of studied GE/α-Bi_2O_3 electrode. Another interesting result appears on Figures 4b and 4c, where it is possible to see the interference of α-Bi_2O_3 on the nucleation of PPy deposits. The PPy coating on GE surface consisted of irregular structures deposits, while in the case of GE/α-Bi_2O_3@PPy electrode (Figure 4c) it is possible to observe structures quite different from Figures 4a and 4b. In fact, the PPy deposits on GE/α-Bi_2O_3 (Figure 4c) by aggregation of several nanometric PPy particles, also with spheroidal shape, unlike the plates detected in Figure 4b.

To demonstrate that the SEM image of GE/α-Bi_2O_3@PPy effectively contains α-Bi_2O_3 particles covered by PPy, it was also collected the energy-dispersive X-ray spectroscopy (EDS) spectra of the electrode (Figure 5), and carried out TEM analysis of material extracted from GE substrate. Clearly, the Figure 5 allows to detect presence of the elements Bi (pink) and O (orange) of α-Bi_2O_3 under PPy layer, which are recognized by C (purple) and N (yellow). Figure 5 shows, as well, the elements K^+ (dark green) and Cl^- (green) from the electrolyte, which were incorporated into the polymer matrix to neutralize the positive charge density of the PPy nitrogen.

To understand the kind of core-shell structure present into GE/α-Bi_2O_3@PPy composite, the Figure 6 is shown. It was found in the TEM grid predominantly nanometric particles of α-Bi_2O_3@PPy. The presence of an irregular PPy granular layer growth covering the surface of α-Bi_2O_3 (dark spot) is resulting from non-uniform current distribution on surface of α-Bi_2O_3 due to the aggregation of grains. As a matter of fact, the thickness of PPy layer electrodeposited on GE/α-Bi_2O_3 occurred not in uniform mode as also detected by Raman characterization. Hence, the studied GE/α-Bi_2O_3@PPy electrode can be defined as an irregular core-shell structure.

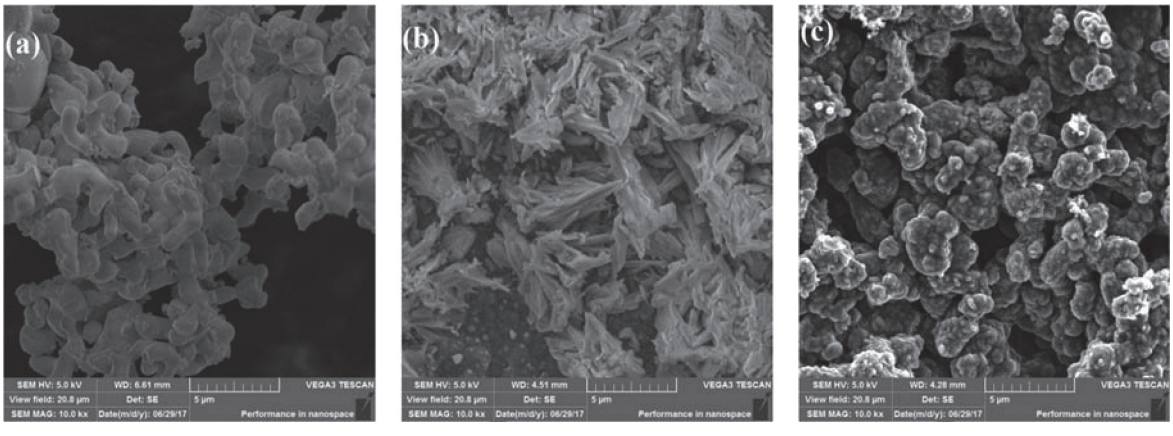

Figure 4. SEM images of the (a) GE/α-Bi_2O_3, (b) GE/PPy, and (c) GE/α-Bi_2O_3@PPy electrodes.

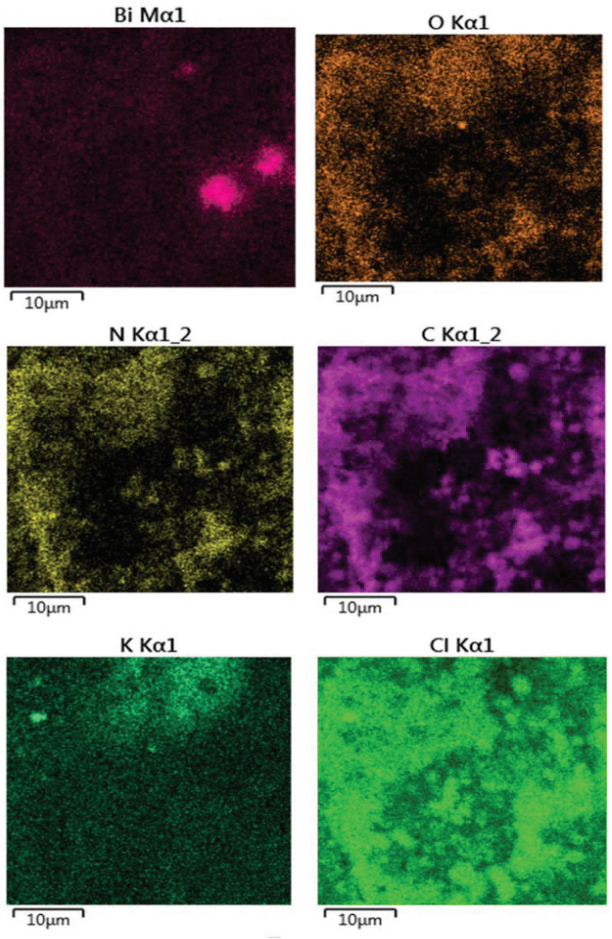

Figure 5. EDS spectra of the GE/α-Bi_2O_3@PPy electrode.

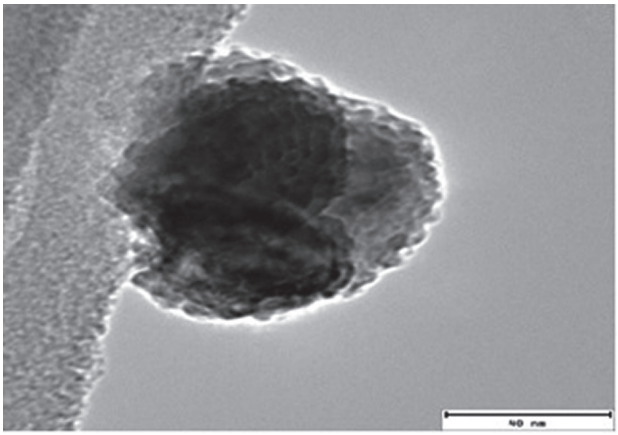

Figure 6. HRTEM picture of GE/α-Bi_2O_3@PPy grains extracted from surface of studied GE/α-Bi_2O_3@PPy electrode.

Electrochemical performance measurement by CV and GCD

The electrochemical performances of the GE/PPy, GE/α-Bi_2O_3, and GE/α-Bi_2O_3@PPy electrodes were analyzed by CV in aqueous 1 mol L^{-1} Na_2SO_4 from –0.30 to 0.70 V *vs.* $Ag_{(s)}/AgCl_{(s)}/Cl^-_{(aq)}$. Figure 7 shows the CV curves recorded for the GE/α-Bi_2O_3, GE/PPy, and GE/α-Bi_2O_3@PPy electrodes. The curves confirmed the capacitive profile of all the materials due to formation of an electric double layer (2 × Na^+ and × SO_4^{2-}) on the electrode surface.

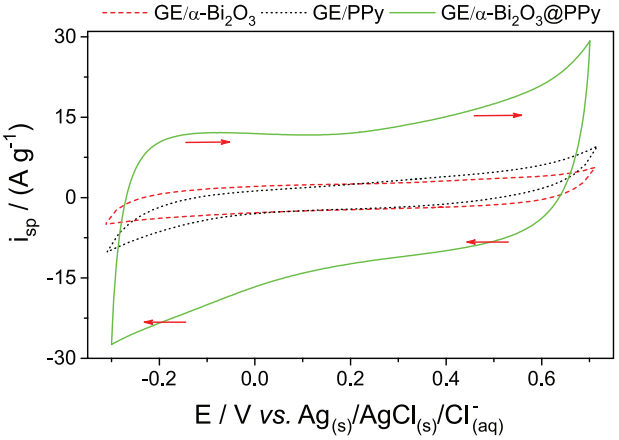

Figure 7. Cyclic voltammograms of characterization of the GE/α-Bi_2O_3, GE/PPy, and GE/α-Bi_2O_3@PPy electrodes in 1 mol L^{-1} Na_2SO_4, recorded at 25 mV s^{-1}.

The CV curve of the GE/α-Bi_2O_3@PPy electrode revealed higher total charge (55.60 mC at 25 mV s^{-1}) as compared to the GE/α-Bi_2O_3 (10.65 mC) and GE/PPy (19.50 mC) electrodes. The highest total charge was obtained for GE/α-Bi_2O_3@PPy electrode due to the α-Bi_2O_3 to have favored the redox processes of PPy by the supply of 4 electrons and 6 H^+, displaying the electronic conductivity.

Figures 8 and 9 show the discharge/charge cycles of GE/α-Bi_2O_3, GE/PPy, and GE/α-Bi_2O_3@PPy electrodes under galvanostatic conditions at different gravimetric current densities.

According to the galvanostatic tests, the GE/α-Bi_2O_3@PPy electrode supported the same current density for a longer time as compared to the GE/α-Bi_2O_3 electrode, which suggested that PPy contributed predominantly to the energy storage and electronic conductivity of the GE/α Bi_2O_3@PPy electrode, due to the cooperation between the double layer capacitance of GE and pseudo-capacitance of the PPy.

In addition, it should be noted that the coating of the α-Bi_2O_3 particles by PPy resulted in an increase of the electroactive area, which intensified the capacitance values of this material. CV curves were integrated and the galvanostatic tests performed to calculate the specific capacitances (Table 3).

The GE/α-Bi_2O_3@PPy electrode presented superior specific capacitances compared to the GE/PPy and GE/α-Bi_2O_3 electrodes. These results corroborated with the morphological and structural analyses of the GE/α-Bi_2O_3@PPy electrode: the α-Bi_2O_3 redox process

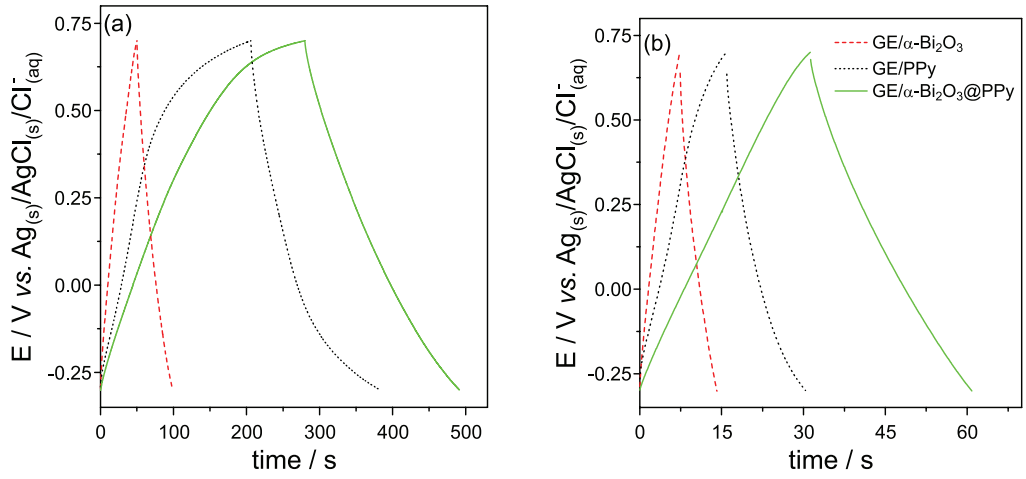

Figure 8. Charge/discharge curves of the GE/α-Bi_2O_3 (red dashed line), GE/PPy (black dotted line) and GE/α-Bi_2O_3@PPy (green solid line) electrodes in 1 mol L^{-1} Na_2SO_4 at (a) 3 A g^{-1} and (b) 10 A g^{-1}, with average mass of 0.10 mg.

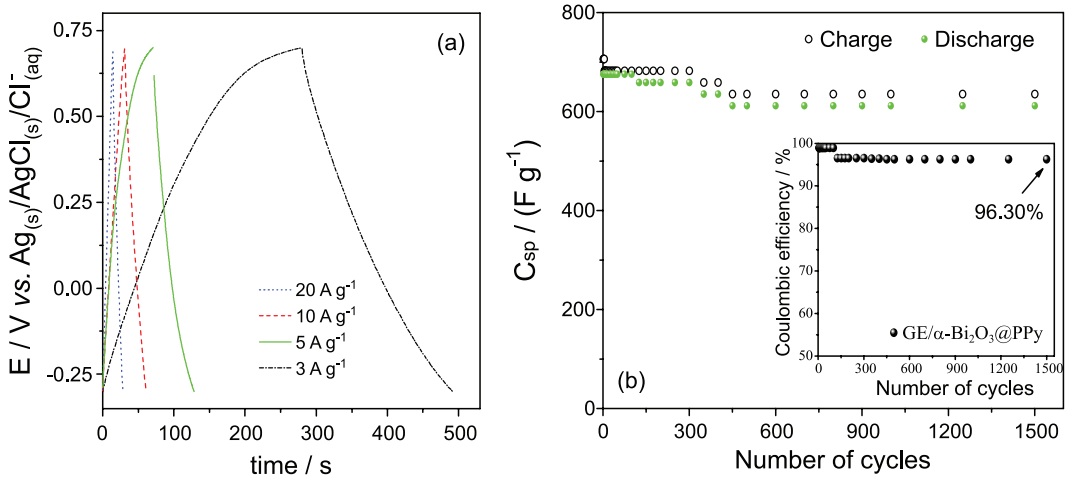

Figure 9. Galvanostatic characterization of GE/α-Bi_2O_3@PPy in 1 mol L^{-1} Na_2SO_4 at different gravimetric current: (a) discharge/charge curves at 20 A g^{-1} (blue dotted line), 10 A g^{-1} (red dashed line), 5 A g^{-1} (green solid line) and 3 A g^{-1} (black dashed-dotted line); (b) specific capacitance and coulombic efficiency *vs.* cycle numbers for the GE/α-Bi_2O_3@PPy electrode at 3 A g^{-1} with average mass of 0.10 mg.

Table 3. Specific capacitance and coulomb efficiency of 50th cycle of studied electrodes in 1 mol L^{-1} Na_2SO_4 between –0.30 and 0.70 V *vs.* $Ag_{(s)}/AgCl_{(s)}/Cl^-_{(aq)}$ at different current densities

Electrode	Current density / (A g^{-1})	C_{sp} / (F g^{-1})	C_{sp} standard deviation[a]	Coulomb efficiency / %
GE/α-Bi_2O_3	3.0	146.55	4.96	98.28
	10.0	71.73	3.42	96.37
GE/PPy	3.0	530.25	7.15	92.45
	10.0	154.55	0.92	93.89
GE/α-Bi_2O_3@PPy	3.0	634.20	6.50	96.30
	10.0	301.90	1.70	96.41

[a]Of three measurements. C_{sp}: specific capacitance; GE: graphite electrode; PPy: polypyrrole.

favored PPy polymeric chain protonation during the electrochemical tests, increasing the PPy conductivity in the hybrid material.

On the basis of electrochemical tests the GE/α-Bi_2O_3@PPy electrode presented the highest increase in specific capacitance in relation to the increment in current, which suggested that the PPy coating on the α-Bi_2O_3 surface provided 650.05 F g^{-1} at 25 mV s^{-1} and ca. 301 F g^{-1} at 10 A g^{-1}. The specific capacitance of PPy increases about 95% on surface of α-Bi_2O_3 when compared to PPy/GE electrode, which suggests that α-Bi_2O_3 would be a very interesting oxide to improve the performance of PPy. In fact, in the case of PPy@TiO_2 prepared by PPy chemical deposition on surface of TiO_2, specific capacitance of about 180 F g^{-1} has been observed, and in the case of PPy@TiN nanotubes and PPy/TiO_2 nanotubes, specific capacitances of 459 and 72 F g^{-1} at 15 A g^{-1}, respectively, have been observed.[29,35]

EIS measurements were carried out from 10 MHz to 100 mHz under open circuit potential. Figure 10a shows the Nyquist plots of the GE/α-Bi_2O_3, GE/PPy, and GE/α-Bi_2O_3@PPy electrodes.

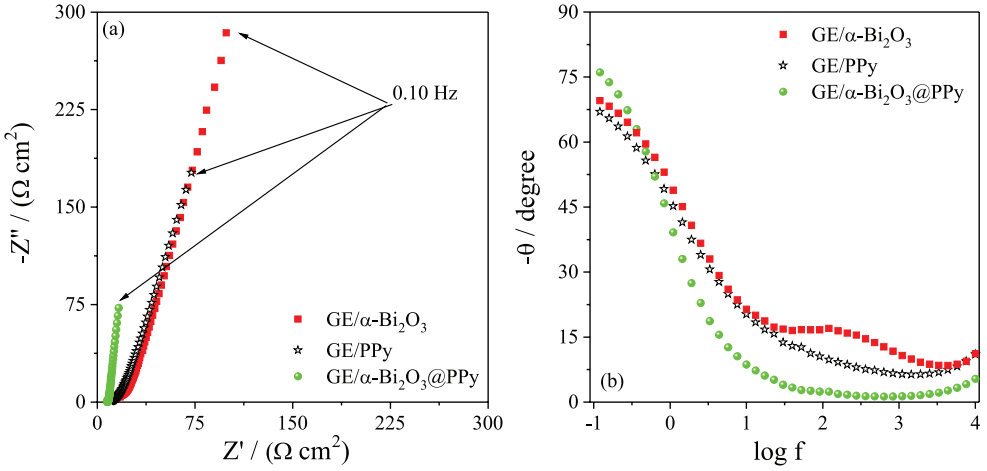

Figure 10. (a) Nyquist diagrams and (b) Bode plots of GE/α-Bi_2O_3, GE/PPy, and GE/α-Bi_2O_3@PPy electrodes in aqueous 1 mol L^{-1} Na_2SO_4, in the range from 10^4 to 10^{-1} Hz at open circuit potential.

The Nyquist diagrams of the GE/α-Bi_2O_3@PPy electrode showed a predominantly capacitive profile (Figure 10a) with lower impedance values as compared to the impedance of the GE/α-Bi_2O_3 and GE/PPy electrodes, indicating that PPy, synthesized on the α-Bi_2O_3, was in its conductive form and, therefore, the positive charge density of the nitrogen had been neutralized by the chloride ions from the electrolyte, thus characterizing a pseudocapacitance.

Bode plots (Figure 10b) show that GE/α-Bi_2O_3@PPy electrode has an electrochemical behavior very similar to the PPy, however, these Bode diagrams revealed increased phase angle for the GE/α-Bi_2O_3@PPy electrode at lower frequencies, as well as the disappearance of the second phase angle assigned to the α-Bi_2O_3, indicating a complete cover of α-Bi_2O_3 by PPy, as detected in HRTEM analysis. Besides, it was possible to verify that the charge storage occurs at low frequencies related to charge accumulation in the bulk of the electrode (limit capacitance).

The PPy-α-Bi_2O_3 hybrid composite is effectively a core-shell structure, where n-p junction is present. The α-Bi_2O_3 core changes the width of charge distribution within the PPy layer grown on its surface, which explains the specific capacitance behavior observed in the present work. Thus, the different specific capacitances of core-shell GE/α-Bi_2O_3@PPy and GE/PPy electrodes can be attributed not only to differences in the PPy electroactive area.

Conclusions

Bi_2O_3 is a transition oxide with good properties. Its association with PPy can create a composite, which improves the electrochemical behavior of the PPy. The solvothermal synthesis afforded monoclinic α-Bi_2O_3, as confirmed by XRD, which showed that Bi_2O_3 was indexed to the monoclinic structure of α-Bi_2O_3 with space group $P2_1/c$ (JCPDS No. 41-1449). SEM, EDS, and Raman characterizations proved that α-Bi_2O_3 was inhomogeneously coated electrochemically with PPy as a core-shell GE/α-Bi_2O_3@PPy hybrid electrode.

The increase in the anodic current density values and consequently the highest charges were obtained for the α-Bi_2O_3@PPy electrode due to the α-Bi_2O_3 having favored the redox processes of PPy by the supply of 4 electrons and 6 H^+. Besides, it was noted that the coating of the α-Bi_2O_3 particles by PPy resulted in an increase of the electroactive area, which intensified the specific capacitance value as compared to the GE/PPy and GE/α-Bi_2O_3 electrodes.

The Bode diagrams revealed increased phase angle for the GE/α-Bi_2O_3@PPy electrode at lower frequencies as well as the disappearance of the second phase angle assigned to the α-Bi_2O_3, indicating a complete cover of α-Bi_2O_3 by PPy. Besides, it was possible to verify that the charge storage occurs at low frequencies related to charge accumulation in the bulk of the electrode (limit capacitance). Therefore, the results indicated that the α-Bi_2O_3@PPy is a promising composite material for application in supercapacitors.

Acknowledgments

This work is a collaboration research project involving members of Rede Mineira de Química (RQ-MG), supported by FAPEMIG (Projects APQ-02249-14 and APQ-03219-14), CAPES, CNPQ and FAPESP (2017/04759-2). The authors also thank the Brazilian Nanotechnology National Laboratory-LME for providing the HRTEM for TEM analysis.

References

1. Li, C.; Balamurugan, J.; Thanh, T. D.; Kim, N. H.; Lee, J. H.; *J. Mater. Chem. A* **2017**, *5*, 397.
2. Chen, J.; Huang, Y.; Li, C.; Chen, X.; Zhang, X.; *Appl. Surf. Sci.* **2016**, *360*, 534.
3. Zhou, H.; Zou, X.; Zhang, Y.; *Electrochim. Acta* **2016**, *192*, 259.
4. Pan, C.; Lv, Y.; Gong, H.; Jiang, Q.; Miao, S.; Liu, J.; *RSC Adv.* **2016**, *6*, 17415.
5. Li, W.; Ji, J.; Cui, X.; Chen, J.; Liu, D.; Deng, H.; Fu, Q.; *Chem. Commun.* **2015**, *51*, 7669
6. Yao, W.; Zhou, H.; Lu, Y.; *J. Power Sources* **2013**, *241*, 359.
7. Li, J.; Wu, Q.; Zan, G.; *Eur. J. Inorg. Chem.* **2015**, *2015*, 5751.
8. Senthilkumar, S. T.; Selvan, R. K.; Ulaganathan, M.; Melo, J. S.; *Electrochim. Acta* **2014**, *115*, 518.
9. Huang, X.; Zhang, W.; Tan, Y.; Wu, J.; Gao, Y.; Tang, B.; *Ceram. Int.* **2016**, *42*, 2099.
10. Brezesinski, K.; Ostermann, R.; Hartmann, P.; Perlich, J.; Brezesinski, T.; *Chem. Mater.* **2010**, *22*, 3079.
11. Farsi, H.; Moghiminia, S.; Roohi, A.; Hosseini, S.-A.; *Electrochim. Acta* **2014**, *148*, 93.
12. Su, H.; Cao, S.; Xia, N.; Huang, X.; Yan, J.; Liang, Q.; Yuan, D.; *J. Appl. Electrochem.* **2014**, *44*, 735.
13. Song, H.; Cai, K.; Wang, J.; Shen, S.; *Synth. Met.* **2016**, *211*, 58.
14. Maia, D. J.; De Paoli, M. A.; Alves, O. L.; Zarbin, A. J. G.; das Neves, S.; *Quim. Nova* **2000**, *23*, 204.
15. Zhou, H.; Han, G.; Xiao, Y.; Chang, Y.; Zhai, H. J.; *Synth. Met.* **2015**, *209*, 405.
16. Hu, J.; Li, M.; Lv, F.; Yang, M.; Tao, P.; Tang, Y.; Liu, H.; Lu, Z.; *J. Power Sources* **2015**, *294*, 120.
17. Yang, C.; Zhang, L.; Hu, N.; Yang, Z.; Wei, H.; Wang, Y.; Zhang, Y.; *Appl. Surf. Sci.* **2016**, *387*, 666.
18. de Oliveira, A. H. P.; de Oliveira, H. P.; *J. Power Sources* **2014**, *268*, 45.
19. Davoglio, R. A.; Biaggio, S. R.; Rocha-Filho, R. C.; Bocchi, N.; *J. Power Sources* **2010**, *195*, 2924.
20. Kumar, N. A.; Baek, J.-B.; *Chem. Commun.* **2014**, *50*, 6298.
21. Meng, F.; Fang, Z.; Li, Z.; Xu, W.; Wang, M.; Liu, Y.; Zhang, J.; Wang, W.; Zhao, D.; Guo, X.; *J. Mater. Chem. A* **2013**, *1*, 7235.
22. Yamazaki, S.; Ito, T.; Murakumo, Y.; Naitou, M.; Shimooka, T.; Yamagata, M.; Ishikawa, M.; *J. Power Sources* **2016**, *326*, 580.
23. Luan, X.; Jiang, J.; Yang, Q.; Chen, M.; Zhang, M.; Li, L.; *Environ. Eng. Manage. J.* **2015**, *14*, 703.
24. Holland, T. J. B.; Redfern, S. A. T.; *Mineral. Mag.* **1997**, *61*, 65.
25. *PeakFit*, version 4.12; Systat Software Inc., San Jose, California, USA, 2003.
26. Wang, Y.; Li, S.; Xing, X.; Huang, F.; Shen, Y.; Xie, A.; Wang, X.; Zhang, J.; *Chem. - Eur. J.* **2011**, *17*, 4802.
27. Saravanan, K.; Reddy, M. V.; Balaya, P.; Gong, H.; Chowdari, B. V. R.; Vittal, J. J.; *J. Mater. Chem.* **2009**, *19*, 605.
28. Gotić, M.; Popović, S.; Musić, S.; *Mater. Lett.* **2007**, *61*, 709.
29. Nguyen, T. T.; Duong, N. H.; *J. Nanomater.* **2016**, *2016*, 6.
30. Vigmond, S. J.; Ghaemmaghami, V.; Thompson, M.; *Can. J. Chem.* **1995**, *73*, 1711.
31. Pereira, A. L. J.; Gomis, O.; Sans, J. A.; Pellicer-Porres, J.; Manjón, F. J.; Beltran, A.; Rodríguez-Hernández, P.; Muñoz, A.; *J. Phys.: Condens. Matter* **2014**, *26*, 225401.
32. Alshareef, H. N.; Chen, W.; Rakhi, R. B.; Hu, L.; Xie, X.; Cui, Y.; *Nano Lett.* **2011**, *11*, 5165.
33. Du, H.; Xie, Y.; Xia, C.; Wang, W.; Tian, F.; *New J. Chem.* **2014**, *38*, 1284.
34. Liu, Y. C.; Hwang, B. J.; *Synth. Met.* **2000**, *113*, 203.
35. Wu, X.; Wang, Q.; Zhang, W.; Wang, Y.; Chen, W.; *Ceram. Int.* **2016**, *42*, 15077.

Submitted: May 18, 2018
Published online: September 27, 2018